Heterogeneous ice nucleation on particles composed of humic-like substances impacted by O_3

Bingbing Wang[1] and Daniel A. Knopf[1]

[1] Heterogeneous ice nucleation plays important roles in cirrus and mixed-phase cloud formation, but the efficiency of organic particles to act as ice nuclei (IN) is still not well understood. Furthermore, the effect of particle oxidation by O_3 on corresponding IN efficiencies has not yet been sufficiently assessed. We present heterogeneous ice nucleation on kaolinite, Suwannee River standard fulvic acid (SRFA), and leonardite standard humic acid particles as a function of particle temperature (T_p), relative humidity with respect to ice (RH_{ice}), nucleation mode, and O_3 exposure. Ice nucleation and water uptake were studied for $T_p > 203$ K and RH_{ice} up to water saturation using a novel ice nucleation apparatus. This study shows that SRFA, leonardite, and corresponding O_3-exposed particles can nucleate ice via different modes at relevant atmospheric conditions. These particles nucleated ice via deposition mode at $T_p \leq 231$ K, and for higher T_p water was taken up or ice was nucleated via deposition or immersion mode. Oxidation of leonardite and SRFA particles by O_3 led to a decrease in deposition nucleation efficiency and to water uptake at lower temperatures for the former and to an increase in the lowest temperature at which deposition nucleation was observed for the latter. Activated IN fractions and heterogeneous ice nucleation rate coefficients (J_{het}) were derived, and corresponding contact angles (θ) were calculated. A parameterization of θ as a function of RH_{ice} is presented which allows derivation of J_{het} for various deposition IN and corresponding ice crystal production rates for application in cloud-resolving models.

1. Introduction

[2] Aerosol particles can affect the global radiative budget directly by scattering and absorption of solar and terrestrial radiation but also indirectly by aerosol-cloud interactions which can lead to the formation of new clouds and modification of the radiative properties of existing clouds [*Twomey*, 1974; *Albrecht*, 1989; *Baker*, 1997; *Rosenfeld*, 2000; *Ramanathan et al.*, 2001; *Forster et al.*, 2007; *Baker and Peter*, 2008]. Aerosol-cloud interactions pose one of the largest uncertainties in prediction of future climate changes [*Forster et al.*, 2007]. The strength of the aerosol indirect effect depends on the efficiency of the aerosol particles to act as cloud condensation nuclei (CCN) and ice nuclei (IN). Whereas an increasingly improved understanding of the role of CCN on climate is being achieved [e.g., *Ramanathan et al.*, 2001; *Lohmann and Feichter*, 2005; *McFiggans et al.*, 2006; *Forster et al.*, 2007], the effect of IN on the atmosphere is still insuffi-

ciently understood [*Baker*, 1997; *Cantrell and Heymsfield*, 2005; *Forster et al.*, 2007; *Baker and Peter*, 2008].

[3] Ice crystals can form by homogeneous or heterogeneous ice nucleation [*Pruppacher and Klett*, 1997]. Homogeneous ice nucleation proceeds from supercooled aqueous particles at temperatures below ~235 K. Heterogeneous ice nucleation can be initiated by a preexisting aerosol particle, the IN, via four modes: deposition mode (the IN nucleates ice directly from supersaturated water vapor), immersion freezing (the IN immersed in a supercooled aqueous droplet nucleates ice), condensation freezing (ice nucleates during water vapor condensation onto the IN), and contact freezing (ice formation is induced by collision of supercooled droplets with IN) [*Vali*, 1985; *Pruppacher and Klett*, 1997]. Heterogeneous ice nucleation occurs at warmer temperatures and lower supersaturations with respect to ice than homogeneous ice nucleation [*Pruppacher and Klett*, 1997] and hence renders IN an important role in atmospheric ice formation.

[4] Atmospheric IN can initiate ice nucleation resulting in the formation of cirrus and mixed-phase clouds. Cirrus clouds can account for one third of the global cloud coverage and play an important role in regulating radiative fluxes [*Wylie et al.*, 2005]. These ice clouds can have a predominant warming effect [*Hartmann et al.*, 1992; *Chen et al.*, 2000; *Choi and Ho*, 2006; *Lee et al.*, 2009]. The radiative properties of cirrus clouds are determined in part by the underlying ice

[1]Institute for Terrestrial and Planetary Atmospheres, School of Marine and Atmospheric Sciences, State University of New York at Stony Brook, Stony Brook, New York, USA.

nucleation mechanisms which can affect the numbers and shapes of the ice crystals [Lynch et al., 2002; Bailey and Hallett, 2004; Wendisch et al., 2007]. In mixed-phase clouds, which consist of supercooled liquid droplets and ice crystals, heterogeneous ice nucleation is the only pathway for ice initiation. This in turn defines the degree of cloud glaciation with subsequent consequences for precipitation and the hydrological cycle [Baker, 1997; McFarquhar et al., 2007; Verlinde et al., 2007; Avramov and Harrington, 2010]. Mixed-phase clouds have also been identified to have a large climatic effect in the polar regions [Curry et al., 1996; Vavrus, 2004; Prenni et al., 2007; Verlinde et al., 2007]. For these reasons a better understanding of the underlying mechanisms governing heterogeneous ice nucleation is needed to evaluate the role of cirrus clouds and mixed-phase clouds on the global radiative budget and hydrological cycle.

[5] Field measurements have shown that organic particles can reach altitudes where temperatures favor ice formation [Murphy et al., 1998; Jost et al., 2004; Murphy et al., 2007; Froyd et al., 2010]. Previous studies also have shown that polar mixed-phase clouds were impacted by carbonaceous particles from biomass burning [Prenni et al., 2009]. Ice crystal observations indicate that IN residues for cirrus and mixed-phase clouds contain some organic material in some instances [Chen et al., 1998; DeMott et al., 2003; Cziczo et al., 2004; Froyd et al., 2010; Prenni et al., 2009]. Recently it has been shown that also anthropogenically emitted organic-containing particles can act as efficient IN under conditions for cirrus cloud formation [Knopf et al., 2010]. A class of organic material extracted from atmospheric aerosol particles, termed humic-like substances (HULIS), consists of a water soluble and an alkaline soluble fraction. Water soluble HULIS can contribute up to 60% to the aerosol water soluble organic carbon [Facchini et al., 1999; Li et al., 2000; Krivacsy et al., 2001; Cavalli et al., 2004; Kiss et al., 2005; Graber and Rudich, 2006; Feczko et al., 2007]. Alkaline soluble HULIS can contribute about 30 to 70% to total HULIS [Feczko et al., 2007; Salma et al., 2008; Baduel et al., 2009]. Suggested sources of HULIS include primary terrestrial sources, biomass burning, secondary organic aerosol formation, and marine sources [Facchini et al., 1999; Decesari et al., 2002; Jang et al., 2002; Mayol-Bracero et al., 2002; Cavalli et al., 2004; Hung et al., 2005; Kiss et al., 2005; Graber and Rudich, 2006; Feczko et al., 2007; Lukács et al., 2007; Lin et al., 2010a, 2010b]. HULIS consist of polycarboxylic acids and resemble to some part terrestrial and aquatic humic substances and fulvic acids [Graber and Rudich, 2006]. Previous aerosol studies employed commercially available fulvic acid and humic acid, such as Suwannee River standard fulvic acid (SRFA) and leonardite, as surrogates of atmospheric HULIS to investigate particle properties such as growth factors and CCN properties [Chan and Chan, 2003; Brooks et al., 2004; Gysel et al., 2004; Svenningsson et al., 2006]. Only few studies have investigated the ice nucleation efficiency of HULIS. Kanji et al. [2008] showed that humic acid sodium salt and leonardite can nucleate ice via deposition mode but this study was limited to 233 K. Fornea et al. [2009] observed that Pahokee peat soil, a humic acid from agricultural soil, are efficient IN in contact freezing mode.

[6] During transport in the atmosphere, the organic particles will interact with atmospheric oxidants such as O_3, NO_3, and OH leading to oxidation of the organic material by heterogenous reactions [Kanakidou et al., 2005; Rudich et al., 2007]. This process, also known as chemical aging, can change the particle's composition and thus its chemical and physical properties [Rudich, 2003; Knopf et al., 2005; Kanakidou et al., 2005; Knopf et al., 2006; Rudich et al., 2007]. Particle oxidation may affect the particle's IN efficiency. Only one study so far has investigated the effect of particle oxidation by gas phase O_3 on ice nucleation [Dymarska et al., 2006]. In the other ice nucleation studies particles were chemically aged by exposure to liquid oxidative agents such as hydrogen peroxide [Garten and Head, 1964], and nitric and sulfuric acid mixtures [Koehler et al., 2009]. Clearly, more experiments are needed to assess if particle oxidation results in a significant impact on the ice nucleation efficiency of organic particles.

[7] In this study, we chose SRFA and leonardite to generate particles serving as surrogates of atmospheric HULIS-containing particles representative of different sources such as biomass burning and marine sources. These organic proxies contain functional groups such as carboxylic and hydroxyl groups which have certain similarities compared to atmospheric HULIS [Graber and Rudich, 2006; Rudich et al., 2007]. SRFA is a water soluble organic compound extracted from a Suwannee River water sample and leonardite is a water insoluble (alkali soluble) humic acid produced by the natural oxidation of exposed lignite [Brooks et al., 2004; Dinar et al., 2006]. Validation of the new experimental setup was performed by determining the IN efficiency of kaolinite particles, a clay mineral, known to be efficient IN. We determined the IN efficiency of SRFA and leonardite particles as a function of T_p, RH_{ice}, nucleation mode, and O_3 exposure.

2. Experimental Method

2.1. Particle Generation

[8] Micrometer-sized particles of kaolinite, SRFA, and leonardite were investigated as potential IN. The particles were dry deposited onto a hydrophobically coated glass plate (for the remainder of the manuscript referred to as substrate) from a tip of a syringe using ultra high-purity N_2 gas as carrier gas. The hydrophobic coating (a monolayer of dichlorodimethylsilane) renders any effect of the substrate on ice nucleation negligible [Koop et al., 1998; Knopf and Koop, 2006; Knopf and Lopez, 2009]. The diameters of the deposited particles were less than 10 μm, with a mean diameter of 1.7–4.3 μm as determined using an optical microscope (OM). All particle samples were prepared in a clean bench (<0.04 particles cm^{-3}) to avoid sample contamination by ambient particles [Knopf and Lopez, 2009]. Table 1 summarizes the range of average particle sizes, numbers, and total surface areas of the various particles samples employed in this study.

2.2. Ice Nucleation Apparatus

[9] Heterogeneous ice nucleation was studied using a custom-built apparatus consisting of an OM and an ice nucleation cell (INC) with an inside volume smaller than 0.8 cm^3 as shown in Figure 1a, based on previously developed setups [Knopf et al., 2002; Dymarska et al., 2006; Knopf and Koop, 2006; Knopf and Lopez, 2009; Knopf

Table 1. The Range of Average Particle Size, Number, Total Surface Area, and IN-Activated Fraction for the Particle Samples of Each Particle Type[a]

Particle Type	Size Mean ± 1σ (μm)	Number	Surface Area ($\times 10^{-4}$ cm^2)	IN-Activated Fraction (%)
Kaolinite	(2.3–4.3)±2.0	660–8500	1.3–7.9	0.01–0.3
SRFA	(2.0–2.4)±1.0	2350–5350	1.4–3.8	0.02–0.13
O$_3$-exposed SRFA	(2.4–2.9)±1.4	1900–5300	2.0–7.3	0.02–0.16
Leonardite	(1.7–3.3)±1.0	2880–10500	3.5–6.4	0.01–0.1
O$_3$-exposed leonardite	(2.0–2.3)±1.1	7300–12600	7.1–8.8	0.008–0.04

[a]The uncertainty in size represents 1 standard deviation.

et al., 2010]. This ice nucleation apparatus allows the exposure of aerosol particles to particle temperatures (T_p) as low as 200 K and RH_{ice} up to water saturation.

[10] The INC was made out of high-density polyethylene to minimize water adsorption which could lead to inhomogeneities of the water vapor field inside the INC. A flow diffuser was also placed in the INC to enhance mixing of the humidified gas. Independent experiments showed that deliquescence of ammonium sulfate particles, water condensa-tion, and evaporation of water droplets occurred equally in each case across the sample area corroborating a homoge-neous water vapor field within the INC. The OM coupled to the INC was operated in reflected light mode and was equipped with a digital camera and imaging software to monitor and record in situ changes in particle phase and size. The entire particle sample area was digitally monitored. The particle samples were placed onto the cooling stage within the INC. The temperature of the cooling stage was
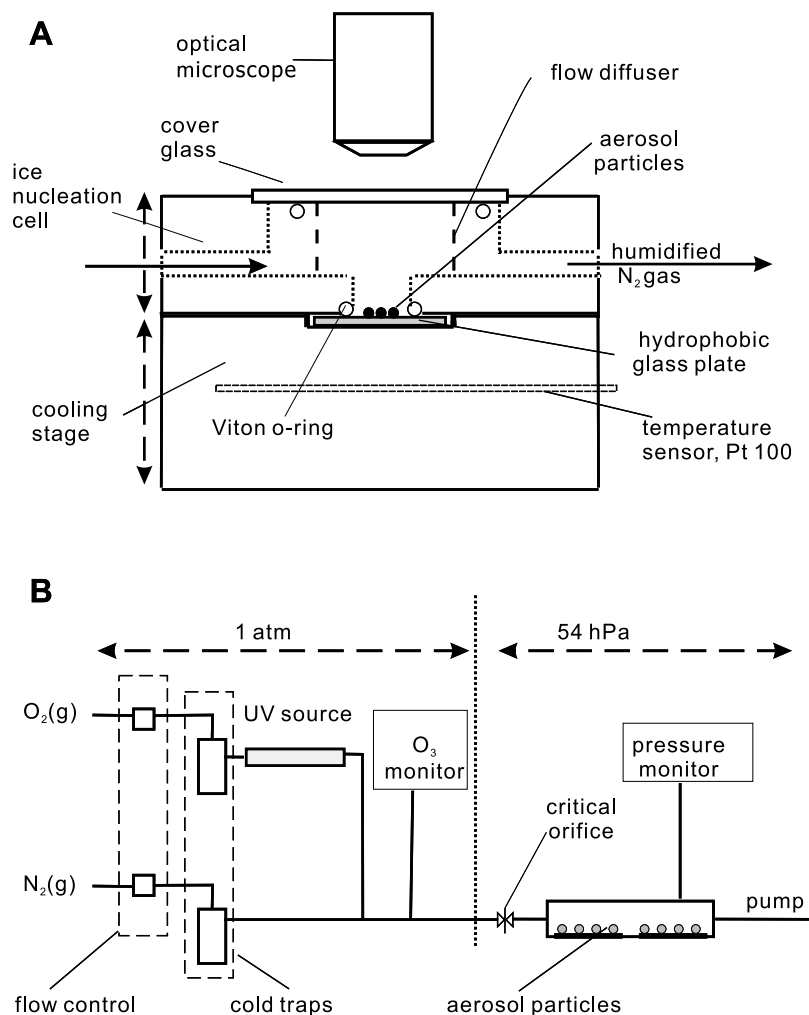
Figure 1. (a) A technical sketch (not to scale) of the ice nucleation cell (INC) coupled to an optical microscope (OM). The outside diameter and the height of the ice nucleation cell are 64 and 14.5 mm, respectively. The dotted lines indicate the INC volume (<0.8 cm^{-3}). (b) The experimental setup for expos-ing particles to O$_3$. O$_3$ generation and quantification were conducted at 1 atm. Aerosol oxidation experi-ments were performed in a flow reactor at 54 hPa.
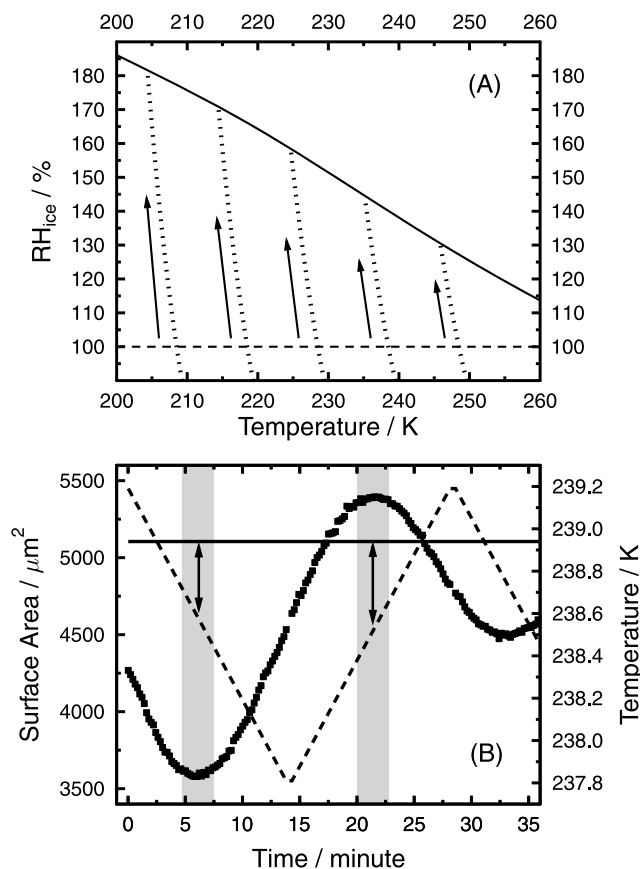
Figure 2. (a) Typical experimental RH_{ice} trajectories. The dashed and solid lines indicate ice saturation and water saturation, respectively. The dotted lines indicate RH_{ice} trajectories for which T_d was constant and T_p was changed by 0.1 K min^{-1}. (b) The changes in surface area and particle temperature during a calibration experiment. The dashed and solid lines represent T_p and T_d, respectively. The black squares represent surface area of one ice crystal determined by OM. The gray bars indicate when the ice crystal maintained a constant surface area. The arrows indicate the deviations between T_p and T_d.

controlled by adjusting the current through a heating foil while maintaining constant cooling by supplying liquid nitrogen. The temperature sensor embedded in the cooling stage was calibrated as described below to yield T_p.

[11] The particles were exposed to a controlled humidified $N_2(g)$ flow of about 1 SLPM (standard liter per minute). The humidified $N_2(g)$ flow was generated by passing $N_2(g)$ through a temperature controlled water reservoir. The $N_2(g)$ used in this study was first passed through a hydrocarbon gas trap and subsequent cold trap at 198 K filled with molecular sieve to minimize contamination by other gas phase species. The presence of a filter with pore size of 0.25 μm in diameter before the gas inlet of the INC did not have a measurable effect on the ice nucleation experiments. The water partial pressure within the humidified $N_2(g)$ was adjusted by changing the temperature of the water reservoir and diluting the humidified flow with a second flow of dry and purified $N_2(g)$. At the exit of the INC the dew point, T_d, was determined using a chilled mirror hygrometer (GE

Sensing) in a range of 203–293 K with an uncertainty of ±0.15 K [*Knopf and Lopez*, 2009; *Knopf et al.*, 2010].

[12] RH_{ice} and relative humidity with respect to water (RH) above the particles were calculated from monitored T_p and T_d using the following equations:

$$RH = \frac{p_{H_2O}^0(T_d)}{p_{H_2O}^0(T_p)}, \tag{1}$$

$$RH_{ice} = \frac{p_{H_2O}^0(T_d)}{p_{H_2O}^{ice}(T_p)}, \tag{2}$$

where $p_{H_2O}^{ice}(T_p)$ and $p_{H_2O}^0(T_p)$ are the saturation vapor pressures over ice and water at T_p, respectively. $p_{H_2O}^0(T_d)$ is the saturation vapor pressure at T_d representing the water partial pressure in the INC. $p_{H_2O}^{ice}(T_p), p_{H_2O}^0(T_p)$, and $p_{H_2O}^0(T_d)$ were calculated using the parameterizations given by *Murphy and Koop* [2005].

2.3. Experimental Procedure

[13] The particles were generated and placed onto the cooling stage within the INC and T_p was set to room temperature. The dew point was adjusted to about 4 K above the temperature at which ice nucleation was to be observed. The particle temperature was then decreased from room temperature to T_d+1 K resulting in RH_{ice} ~88%. The experiment started as T_d was stable for at least 30 min. Then RH_{ice} was continuously increased by cooling T_p with a rate of 0.1 K min^{-1} until ice formation or water uptake was observed [*Dymarska et al.*, 2006; *Eastwood et al.*, 2008]. The cooling rate is relevant to rates associated with updraft speeds reported for midlatitude and low-latitude cirrus clouds [*Kärcher and Ström*, 2003]. Typical experimental RH_{ice} trajectories are illustrated in Figure 2a for different initial T_p. Each dotted line in Figure 2a represents RH_{ice} trajectory for which T_d is constant. The change in RH_{ice} is ~2.3% to 1.5% per minute for temperatures from 200 to 260 K, respectively. As T_p decreases by ~4 K below T_d, RH_{ice} increases from 100% to ~160% and 190% at temperatures of 260 and 200 K, respectively.

[14] Images of the particles were recorded every 0.02 K, i. e., every 12 s, while simultaneously recording the experimental time, T_d, and T_p. The onset of ice nucleation or water uptake by the particles was determined by the change of the particle size and phase from the recorded images. The OM allowed us to visually identify the changes in particle size and phase due to water uptake or ice formation of larger than 0.2 and 1 μm when using a magnification of 1130x and 230x, respectively. Estimates of the water vapor flux indicated that the water vapor supply was sufficient for a detectable size change of the particles by 0.2 and 1 μm due to water uptake or ice formation on deposited particles between 6 and 36 s at 235 K, respectively, assuming a water vapor condensation coefficient of 0.01. At higher temperatures the time needed to establish the detectable size change is significantly faster (i. e. 5 s instead of 36 s) due to a higher water partial pressure. We report ice formation as immersion freezing if water uptake was observed prior to ice crystal formation and as deposition ice nucleation if no water uptake was observed prior to ice crystal formation. Thus, immersion freezing events which occur within <6 and 36 s may be misinterpreted as deposition

nucleation by our system. Here we report ice nucleation onsets, i. e., T_p and RH_{ice} values at which the first ice crystal was observed. In some instances multiple ice crystals formed simultaneously. Then all the initially formed ice crystals were counted. Subsequent ice formation events were discarded since a uniform RH field may not persist when ice crystals are present in the INC.

[15] After an ice nucleation experiment T_p was calibrated following previously applied methods [*Parsons et al.*, 2004; *Dymarska et al.*, 2006; *Eastwood et al.*, 2008] which is outlined below. Prior to repetition of the experiment, the particle sample was warmed up to 275 K to ensure complete sublimation of ice crystals and exclude the possibility of preactivation [*Knopf and Koop*, 2006]. For blank substrates and each particle type, the experiment was repeated at least 3 times for each particle sample employing minimum 3 independent samples for each investigated T_p.

2.4. Calibration

[16] Temperature calibration was conducted following previous methods [*Parsons et al.*, 2004; *Dymarska et al.*, 2006; *Eastwood et al.*, 2008]. T_p was calibrated against T_d by measuring the 2-D projected surface area (SA) of ice crystals. At constant T_d, ice crystals grow or shrink (SA increases or decreases) when T_p is decreased or increased, respectively. A calibration experiment is shown in Figure 2b. At the beginning of the calibration experiment in presence of at least one ice crystal, when T_p is higher than T_d, thus $RH_{ice} < 100\%$, resulting in sublimation of the ice crystal and corresponding decrease in SA. Subsequently, RH_{ice} is increased by decreasing T_p at 0.1 K min^{-1}. When the ice crystal maintains a constant SA as indicated by the gray bar in Figure 2b, $RH_{ice} = 100\%$ indicating that the temperature of the substrate is equal to T_d. Further decrease of T_p results in growth of the ice crystal corresponding to an increase of SA. The determined difference between T_d and T_p represents the temperature offset for which T_p has to be calibrated. The conservative experimental uncertainties were calculated from the uncertainties of $\Delta T_d < \pm 0.15$ K and $\Delta T_p < \pm 0.3$ K resulting in $\Delta RH_{ice} < \pm 11\%$ for 200 K and $\Delta RH_{ice} < \pm 3\%$ for 260 K. Error bars presented for the data in this study indicate on standard deviation of observed RH_{ice} and T_p values or above discussed experimental uncertainties in RH_{ice} and T_p whichever is larger.

2.5. Ozone Exposure System

[17] Atmospheric particle O_3 exposure of ~40 ppb for two weeks was achieved using the flow system shown in Figure 1b. This results in an O_3 exposure of 4.8×10^{-2} atm s which was calculated from the O_3 partial pressure (P_{O3}) and the time particles were exposed to O_3 as $P_{O3} t$ [*Knopf et al.*, 2005, 2006]. To generate O_3, a $N_2(g)$ flow and a $O_2(g)$ flow were first passed through a hydrocarbon gas trap and subsequent cold trap at 198 K for further purification. O_3 was generated by passing the $O_2(g)$ through an ultraviolet source operated at 254 nm (Jelight Inc.) and subsequently mixed with a dry $N_2(g)$ flow. The O_3-containing flow was introduced into a flow reactor consisting of a 35 cm long denuder with inner diameter of 2 cm in which the particle samples or blank substrates were placed. An O_3 monitor (2B Technologies) working at atmospheric pressure was used to measure

inlet gas pressure and the concentration of O_3 every 10 s based on the absorption of UV light by O_3 at 254 nm.

[18] In the laboratory we mimic the atmospheric O_3 exposure by employing a higher O_3 concentration which allows us to reduce the experimental exposure time. The entire system was flushed thoroughly with ultra high-purity $N_2(g)$ before placing the samples inside the flow reactor. The particle samples were exposed to O_3 concentrations of ~85 ppm for 3 h in the flow reactor at 54 hPa. This approach assumes that the O_3 exposure and thus the degree of particle oxidation behaves linearly with O_3 concentration. If oxidation occurs as a second-order or higher reaction order, the efficiency of the heterogeneous oxidation process may change significantly with O_3 concentration and, hence, laboratory O_3 exposure may lead to a different degree of oxidation when compared to the atmospherically relevant one [*Springmann et al.*, 2009]. Volatilization of organic material due to O_3 oxidation, e. g. as observed for the reaction of O_3 with liquid oleic acid [e.g., *Zahardis and Petrucci*, 2007], cannot be ruled out. However, the primary aim of the laboratory O_3 exposure experiments of SRFA and leonardite particles is to detect any significant effect of heterogeneous oxidation on the particles' ice nucleation efficiency which is detectable under these experimental conditions.

2.6. Chemicals

[19] Kaolinite dust was purchased from Fluka. Leonardite and SRFA were purchased from International Humic Substance Society (IHSS). Millipore water (resistivity ≥ 18.2 MΩ cm) was used for humidification. O_2 (99.99%) and N_2 (99.999%) were purchased from Praxair.

3. Results and Discussion

3.1. Ice Nucleation on Kaolinite Particles

[20] Validation of the novel INC was performed by determining the ice nucleation onsets of kaolinite particles which are known to be efficient IN [*Roberts and Hallett*, 1968; *Schaller and Fukuta*, 1979; *Bailey and Hallett*, 2002; *Dymarska et al.*, 2006; *Eastwood et al.*, 2008]. Before conducting the ice nucleation experiments, the quality of the hydrophobic coating and thus the effect of the substrate on ice nucleation was determined by measuring the ice nucleation onsets of particle free substrates. Figure 3 shows that ice nucleation or water uptake on blank substrates occurred at RH_{ice} from 121% to 168% for temperatures from 251 to 208 K. These RH_{ice} values indicate the experimental maximum achievable RH_{ice} values at corresponding temperatures for which an effect of the substrate on ice nucleation can be ruled out. In other words, ice formation observed at RH_{ice} values lower than the maximum RH_{ice} derived from blank substrates can be attributed to ice nucleation initiated by the deposited particles. The OM technique allowed visual confirmation that ice nucleation was induced by particles and not by the substrate and that at the same time no water condensed on the particle free area of the substrate. As shown in Figure 3, O_3-exposed substrates show similar maximum RH_{ice} values suggesting that O_3 exposure did not significantly affect the quality of the hydrophobic coating for our experimental conditions. This finding is corroborated by a previous study of the photo-reactivity of alkylsiloxane self assembled monolayers
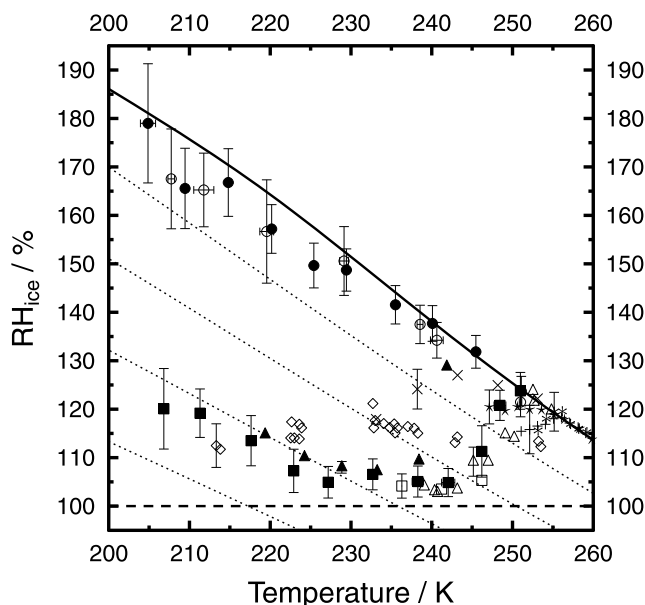
Figure 3. Ice nucleation onset conditions of blank substrates and kaolinite particles. The open and solid circles show the onsets for unexposed and O_3-exposed blank substrates, respectively. The solid squares represent ice nucleation onsets for kaolinite particles. Solid and dashed lines indicate water saturation and ice saturation, respectively. The diagonal dotted lines indicate (top right to bottom left) 90%, 80%, 70%, and 60% RH [*Murphy and Koop*, 2005]. Previous ice nucleation data employing kaolinite are shown as open triangles [*Dymarska et al.*, 2006], open squares [*Eastwood et al.*, 2008], open diamonds [*Bailey and Hallett*, 2002], pluses [*Schaller and Fukuta*, 1979], stars [*Roberts and Hallett*, 1968], solid triangles [*Welti et al.*, 2009], asterisks [*Zimmermann et al.*, 2007], and crosses [*Salam et al.*, 2006]. Corresponding representative error bars are given on the selected data points.

(SAM) on SiO_2 surfaces showing that O_3 did not have a significant effect on the degradation of the monolayer [*Ye et al.*, 2001].

[21] Figure 3 shows the ice nucleation onsets for kaolinite particles as a function of T_p and RH_{ice} observed here and data from previous studies [*Roberts and Hallett*, 1968; *Schaller and Fukuta*, 1979; *Bailey and Hallett*, 2002; *Dymarska et al.*, 2006; *Salam et al.*, 2006; *Zimmermann et al.*, 2007; *Eastwood et al.*, 2008; *Welti et al.*, 2009]. The kaolinite particle sample characteristics are given in Table 1. Our data show that kaolinite particles induced ice formation via deposition mode at 102–124% RH_{ice} for temperatures below 251 K. At 251 K some ice formation events (6 out of 9 experiments) occurred at ~124% RH_{ice} which corresponds to water saturation without indication of water uptake prior to ice formation. For the remaining experiments at 251 K, water uptake was observed first and followed by immersion freezing. *Dymarska et al.* [2006] reported water uptake by kaolinite particles prior to ice formation at 252.5 K. Previous studies also reported the highest temperatures for deposition ice nucleation range from 251 to 254 K [*Roberts and Hallett*, 1968; *Schaller and*

Fukuta, 1979; *Bailey and Hallett*, 2002; *Salam et al.*, 2006; *Zimmermann et al.*, 2007]. The RH_{ice} ice nucleation onset decreased from 124% at 251 K to ~105% at 243–220 K similar to previous studies [*Dymarska et al.*, 2006; *Eastwood et al.*, 2008; *Welti et al.*, 2009] and then increased to 120% at 207 K. Our results corroborate that kaolinite particles are very efficient IN inducing ice nucleation as low as 102% RH_{ice} in agreement with previous studies [*Roberts and Hallett*, 1968; *Schaller and Fukuta*, 1979; *Bailey and Hallett*, 2002; *Dymarska et al.*, 2006; *Salam et al.*, 2006; *Zimmermann et al.*, 2007; *Eastwood et al.*, 2008; *Welti et al.*, 2009].

3.2. Ice Nucleation on SRFA and O_3-Exposed SRFA Particles

[22] Figure 4a shows ice nucleation onsets and water uptake by SRFA and O_3-exposed SRFA particles as a function of T_p and RH_{ice}. The corresponding particle sample characteristics are summarized in Table 1. For $T_p \leq 231$ K, ice nucleated on SRFA particles at mean RH_{ice} values of 137–148% which were well below water saturation and no water uptake was observed indicating that ice nucleation occurred via deposition mode. At 236 and 241 K, ice formation events occurred either via deposition mode or immersion freezing. Water uptake was first observed and followed by immersion freezing for 4 out of 10 experiments and 3 out of 12 experiments at 236 and 241 K, respectively. For the remaining experiments at 236 and 241 K ice nucleated on SRFA particles via deposition mode. At 246 K, all ice formation events occurred via immersion freezing in which water uptake was observed prior to ice nucleation at 98% RH. At 251 K, water uptake was first observed at 99% RH on SRFA particles but only in some cases (3 out of 9 experiments) followed by immersion freezing.

[23] For O_3-exposed SRFA particles, all ice formation events occurred via deposition mode at $T_p \leq 241$ K which is about 10 K warmer compared to SRFA particles. This implies that oxidation by O_3 enhanced the ice nucleation efficiency of the investigated SRFA particles by up to 10 K. For $T_p \leq 231$ K, ice nucleation occurred on O_3-exposed SRFA particles via deposition mode at mean RH_{ice} values of 137–150% which is in a similar range as for SRFA particles. At 246 K, all ice formation events occurred via immersion freezing in which water uptake by O_3-exposed SRFA particles was observed prior to ice nucleation. At 251 K, water uptake was first observed at 98% RH on O_3-exposed SRFA particles but only in some cases (3 out of 12 experiments) followed by immersion freezing.

[24] Water uptake for SRFA and O_3-exposed SRFA particles occurred close to water saturation. This is expected since SRFA particles possess a small growth factor of 1.1 at 90% RH for 295–303 K [*Brooks et al.*, 2004; *Svenningsson et al.*, 2006]. Here, our data suggest that oxidation by O_3 renders SRFA particle surfaces more IN efficient and less favorable to water uptake.

3.3. Ice Nucleation on Leonardite and O_3-Exposed Leonardite Particles

[25] Figure 4b shows ice nucleation onsets and water uptake by leonardite and O_3-exposed leonardite particles as a function of T_p and RH_{ice}. Table 1 lists the corresponding particle sample characteristics. For both leonardite and
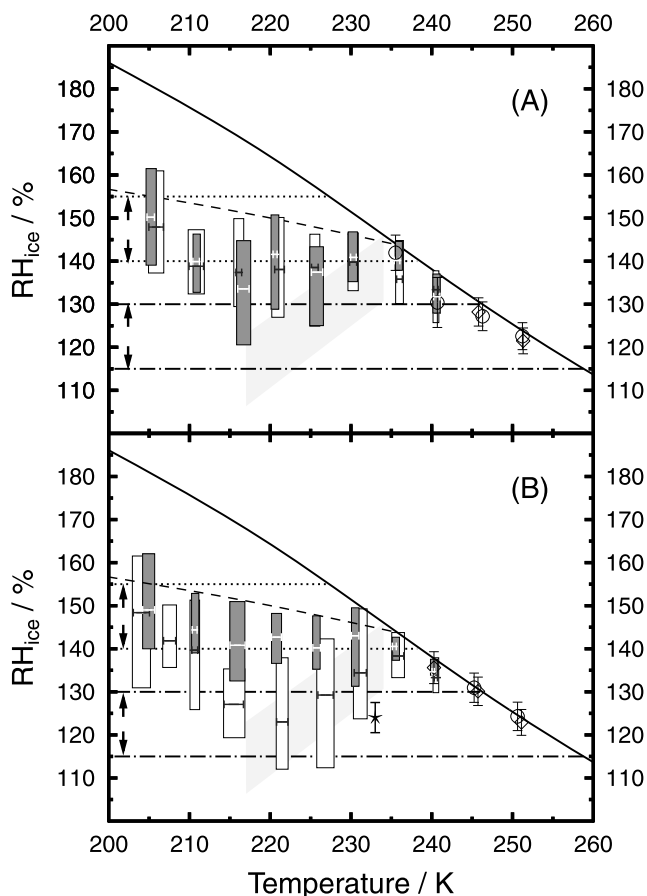
Figure 4. The onset conditions for ice nucleation and water uptake as a function of T_p and RH_{ice} (a) for SRFA and O_3-exposed SRFA particles and (b) for leonardite and O_3-exposed leonardite particles. In Figures 4a and 4b, the white and gray bars show the ranges of observed ice nucleation onsets with mean onset RH_{ice} indicated by the horizontal lines within the bars for deposition ice nucleation on unexposed and O_3-exposed particles, respectively. The open circles and open diamonds indicate the mean onset values of water uptake by unexposed and O_3-exposed particles, respectively. Solid line is the same as in Figure 3. The dashed line represents RH_{ice} thresholds for homogeneous ice nucleation of an aqueous droplet [*Koop et al.*, 2000]. Light gray area indicates bounds of continental cirrus onset formation [*Heymsfield and Miloshevich*, 1995]. RH_{ice} values between horizontal paired dash-dotted and dashed lines indicated by arrows represent the lower limits for cirrus formation conditions in the Northern and Southern hemispheres, respectively [*Ström et al.*, 2003]. The star in Figure 4b represents deposition ice nucleation onset on leonardite particles [*Kanji et al.*, 2008].

O_3-exposed leonardite particles, water uptake occurred at 98% RH for $T_p \geq 246$ K. At 246 K, in some cases initial water uptake was followed by ice formation via immersion freezing on both leonardite and O_3-exposed leonardite samples.

[26] Figure 4b shows that RH_{ice} ice nucleation onsets for leonardite particles possess a strong temperature dependence. Leonardite particles nucleated ice via deposition mode at mean RH_{ice} values of 123–148% for $T_p \leq 241$ K. 14 additional ice nucleation experiments using 2 more independent leonardite particle samples were conducted at 221 and 227 K to further corroborate the observed temperature dependency of the RH_{ice} ice nucleation onsets. We observed significant numbers of ice nucleation events that occurred as low as 112% RH_{ice} for T_p between 221 and 227 K.

[27] O_3-exposed leonardite particles nucleated ice via deposition mode at mean ice nucleation onsets of 140–149% RH_{ice} at $T_p \leq 236$ K. At 241 K, only 40% of the ice formation events (4 out of 10 experiments) occurred via deposition mode. For the remaining experiments at 241 K, ice nucleated via immersion freezing after water uptake at 98% RH. Figure 4b indicates that O_3-exposed leonardite particles nucleated ice in average 10 to 20% RH_{ice} higher compared to unexposed leonardite particles for T_p between 215 and 227 K. Although RH_{ice} ice nucleation onsets for O_3-exposed leonardite particles partly overlap with those for leonardite particles, the data suggest that oxidation by O_3 decreases the IN efficiency of leonardite particles between 215 and 227 K. Leonardite and O_3-exposed leonardite particles can nucleate ice via different modes over a wide temperature range from 204 to 251 K at relevant atmospheric RH_{ice} values.

[28] Few studies investigated the ice nucleation efficiency of HULIS particles [*Fornea et al.*, 2009; *Kanji et al.*, 2008]. *Kanji et al.* [2008] reported that leonardite particles can nucleate ice via deposition mode at 124% RH_{ice} at 233 K which is in agreement with our data within the uncertainties of both studies. It is commonly assumed that the efficiency of IN depends on active sites which can be associated with cracks, cavities, chemical and physical bonds allowing the enhanced interaction with water vapor [*Pruppacher and Klett*, 1997]. Leonardite particles contain both hydrophobic and hydrophilic acids and SRFA particles only contain hydrophobic organic acids as stated by the International Humic Substance Society (http://www.ihss.gatech.edu). The hydrophilic component of leonardite may facilitate the formation of hydrogen bonds with water molecules resulting in more active sites than SRFA. If hydrophilic groups affect ice nucleation, it would be expected that leonardite induces ice nucleation at lower RH_{ice} than SFRA. Our data show that RH_{ice} ice nucleation onsets for leonardite are lower than the ones for SFRA for T_p between 215 and 227 K. Thus, the presence of hydrophilic groups may contribute to the higher ice nucleation efficiency of leonardite particles compared to SRFA particles.

[29] For all investigated particle samples, we did not observe a significant relationship between observed ice nucleation onsets and particle size, number, and surface area. Table 1 summarizes the ranges in particle size, number, and surface area for the various samples investigated here. Table 1 indicates that particle size, number, and surface area remained within 1 order of magnitude. The resulting minor effect on ice nucleation onset is in part corroborated by previous studies indicating that a decrease of the particle loading by 3 orders of magnitude increases the ice nucleation onset from 102 to 115% RH_{ice} and a decrease of total particle surface area by up to 3 orders of magnitude resulted in an increase of the ice nucleation onset by about 10% [*Kanji and Abbatt*, 2006; *Kanji et al.*, 2008]. Thus, potential

changes in corresponding ice nucleation onsets may be well within our experimental uncertainties.

3.4. Effect of Particle Oxidation on Ice Nucleation

[30] Oxidation of organic particles by atmospheric trace gases can lead to the formation of hydrophilic functional groups on the particle surface [*Thomas et al.*, 2001; *Eliason et al.*, 2003; *Molina et al.*, 2004; *Rudich et al.*, 2007; *Knopf et al.*, 2006] that may change the ice nucleation efficiency of the particles. Figure 4a shows that oxidation by O_3 renders SRFA particles more ice nucleation efficient in deposition mode at temperatures between 236 and 241 K. Thus particle oxidation by O_3 may enhance the ice nucleation efficiency of SRFA particles by formation of hydrophilic functional groups. However, below 231 K, RH_{ice} ice nucleation onsets for deposition ice nucleation on O_3-exposed SRFA particles are similar to those for SRFA particles. This suggests that the chemical nature of the surface, such as hydrophilic groups, may not be the only determining factor for ice nucleation.

[31] In the case of leonardite particles, particle oxidation by O_3, however, renders the particles less ice nucleation efficient for the temperature range of 215 to 225 K as shown in Figure 4b. The reason for these changes in IN efficiency is not clear. Leonardite particles can react with ozone with reactive uptake coefficients of 3.8×10^{-6} to 3.7×10^{-5} [*D'Anna et al.*, 2009]. Our data suggest that oxidation of leonardite particles by O_3 results in deactivation of active sites for a specific temperature range. If this is due to a chemical alteration of the particle surface, i. e., changes in chemical bond structures by addition of new hydrophilic sites or replacement of existing sites, or physical alteration, i. e., restructuring of cracks and cavities due to volatilization of organic material, could not be determined with our experimental method.

[32] Only few studies have investigated the effect of oxidation of organic particles on ice nucleation efficiency [*Dymarska et al.*, 2006; *Garten and Head*, 1964; *Koehler et al.*, 2009]. *Garten and Head* [1964] found that oxidation of wood char particles by suspending those in hydrogen peroxide may lead to higher IN efficiency. [*Koehler et al.*, 2009] showed that oxidation of soot particles by immersing particles in concentrated nitric and sulfuric acid mixture may render the soot particle more IN active. *Dymarska et al.* [2006] indicated that oxidation of soot by gas phase O_3 did not have a significant effect on the heterogeneous IN efficiency of soot particles at temperatures above 240 K. The data presented here show that O_3 oxidation can have different impacts on the ice nucleation efficiency of SRFA and leonardite particles. Our data suggest that there is not a clear relationship between particle hydrophilicity and ice nucleation efficiency, and thus other factors may also govern the nucleation process.

3.5. IN-Activated Fraction and Heterogeneous Ice Nucleation Rate Coefficient

[33] Here we report ice nucleation onsets at which the initially formed ice crystals were observed. The OM technique is sensitive to each individual ice nucleation event. Thus, the IN-activated fraction is mainly defined by the number of deposited particles. Table 1 gives the range of

derived IN-activated fractions for the particles samples employed in this study. The IN-activated fractions range from 0.008% to 0.3%. Kaolinite as the most efficient IN investigated in this study exhibits the highest IN-activated fraction.

[34] The experimental ice nucleation data obtained here were employed to derive heterogeneous ice nucleation rate coefficients (J_{het}) which are defined as the number of nucleation events per area of ice nucleus and time ($cm^{-2}\ s^{-1}$). The analysis of the experimental data has been described in detail previously [*Koop et al.*, 1997; *Zobrist et al.*, 2007]. Here we briefly introduce the data analysis. For a given temperature interval (ΔT), different numbers of ice nucleation events may occur. J_{het} as a function of temperature was derived using the following formula

$$J_{het}\left(T^i\right) = \frac{n_f^i}{t_{tot}^i \cdot S^i}, \qquad (3)$$

where $J_{het}\left(T^i\right)$ is the average heterogeneous ice nucleation rate coefficient at the mean freezing temperature of ice nucleation events (T^i) within the ith temperature interval, n_f^i is the number of observed ice nucleation events and t_{tot}^i is the total observation time in the ith temperature interval, and S^i accounts for the particle surface area available for the ice nucleation within the ith temperature interval. The product $t_{tot}^i \cdot S^i$ for the ith temperature interval is given by the sum of the contributions from the samples which remain unfrozen and samples that nucleate ice [*Zobrist et al.*, 2007] according to

$$t_{tot}^i \cdot S^i = \sum_{j=1}^{n_f^i} \left(\frac{T_{st}^i - T_{f,j}^i}{c_r} \right) S_j^i + \frac{\Delta T}{c_r} S_{uf}^i, \qquad (4)$$

where T_{st}^i is the start temperature of the ith temperature interval, $T_{f,j}^i$ is the freezing temperature and S_j^i is the particle surface area available for the jth nucleation event occurring within the ith temperature interval, c_r is the cooling rate applied in the experiments, and S_{uf}^i is the total particle surface area that remain unfrozen until the end of the ith temperature interval. In this study, ΔT of 0.02 K was chosen corresponding to the temperature interval between two sequentially recorded images which allow to discriminate nucleation events. Surface areas were estimated from the number and sizes of the particles deposited on the substrate using OM and assuming the particles have spherical geometry. The particles most likely exhibit nonideal geometry including cracks, cavities, or intrusions. Thus, our assumption will result in an underestimation of the actual particle surface area and yield an upper limit of J_{het}.

[35] Figure 5 presents the derived J_{het} values for deposition ice nucleation for the different particle types studied here as a function of temperature. For all investigated particle types J_{het} is a strong function of temperature as expected from classical nucleation theory (CNT) [*Pruppacher and Klett*, 1997]. Figure 5a shows that J_{het} for SRFA particles increases by 2–3 orders of magnitude within 2 K for the investigated particle temperatures. For example, J_{het} increases from $12\ cm^{-2}\ s^{-1}$ to $940\ cm^{-2}\ s^{-1}$ within 1.2 K from 226.1 K to 224.9 K. Figure 5b presents J_{het} for O_3-exposed
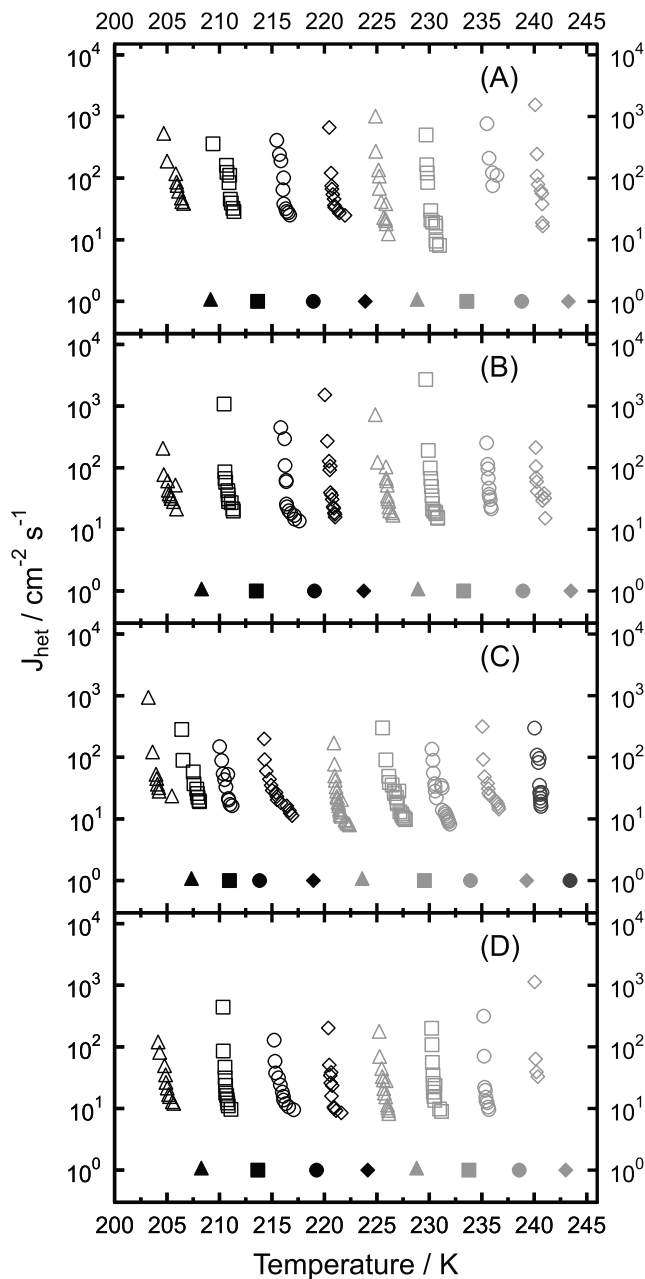
Figure 5. Experimentally derived J_{het} values as a function of temperature for deposition ice nucleation for (a) SRFA, (b) O_3-exposed SRFA, (c) leonardite, and (d) O_3-exposed leonardite particles. Each open symbol type in corresponding gray level represents ice nucleation experiments conducted at same T_d. Solid symbols represent corresponding temperatures at which $RH_{ice} = 100\%$.

SRFA particles. The corresponding maximum of J_{het} ranges from 190 to 2700 cm^{-2} s^{-1} for the observed temperatures. For T_p below 231 K O_3-exposed SRFA particles exhibit similar J_{het} values as for SRFA particles. As shown in Figures 5c and 5d, maximum J_{het} values for leonardite and O_3-exposed leonardite particles range from 140 to 870 cm^{-2} s^{-1} and from 110 to 1130 cm^{-2} s^{-1}, respectively, for the observed temperatures.

3.6. Contact Angle

[36] CNT can be employed to describe heterogeneous nucleation in atmospheric cloud models [e.g., *Kärcher*, 1998; *Morrison et al.*, 2005] and to analyze laboratory data [e.g., *Chen et al.*, 2008; *Eastwood et al.*, 2008; *Kanji and Abbatt*, 2010]. A key parameter in determining IN efficiency is the contact angle (θ). θ for an ice embryo formed on an IN characterizes the relationship of surface free energies among the three involved interfaces including water vapor, ice embryo, and IN. Here, we calculated θ from the experimentally derived J_{het} for the different particle types employed in this study following previous methods [*Eastwood et al.*, 2008; *Kanji and Abbatt*, 2010]. J_{het} is defined as

$$J_{het} = A \cdot \exp\left(\frac{-\Delta F_{g,het}}{kT}\right), \tag{5}$$

where A is a preexponential factor, $\Delta F_{g,het}$ is the free energy of formation of the ice germ, k is the Boltzmann constant, and T is the temperature. Assuming that an ice embryo on a curved solid substrate can be described as a spherical cap, the free energy of ice embryo formation is given by [*Pruppacher and Klett*, 1997]

$$\Delta F_{g,het} = \frac{16\pi M_w^2 \sigma_{i/v}^3}{3[RT\rho \ln S_{ice}]^2} \cdot f(m,x), \tag{6}$$

where M_w is the molecular weight of water, $\sigma_{i/v}$ is the surface tension at the ice-vapor interface, R is the universal gas constant, ρ is the density of ice, S_{ice} is the saturation ratio with respect to a planar ice surface, $f(m, x)$ is the geometric factor, and x is the ratio of the radius of the substrate to the radius of spherical ice germ. m is the compatibility parameter. θ usually is defined by the compatibility parameter, $m = \cos(\theta)$ [*Fletcher*, 1958]. Assuming the radius of the particle substrate is much larger than the radius of the ice germ which is a good approximation for aerosol particles, then $f(m, x)$ is defined, without considering curvature adjustment which is negligible for aerosol sizes >0.1 μm [*Pruppacher and Klett*, 1997; *Chen et al.*, 2008], as follows:

$$f(m) = \frac{m^3 - 3m + 2}{4}. \tag{7}$$

[37] To calculate θ, the free energy of ice germ nucleation was calculated from experimentally derived J_{het} assuming $A = 10^{25}$ cm^{-2} s^{-1} [*Pruppacher and Klett*, 1997; *Eastwood et al.*, 2008; *Kanji and Abbatt*, 2010]. Then, θ was calculated using equations (6) and (7) with $M_w = 18.015$ g mol^{-1}, $\rho = 0.92$ g cm^{-3}, and $\sigma_{i/v} = 106$ mJ m^{-2} [*Pruppacher and Klett*, 1997; *Eastwood et al.*, 2008; *Kanji and Abbatt*, 2010].

[38] The derived θ allows for comparing the IN efficiencies of different particle types. Particles with smaller θ values are more efficient IN. Figure 6a shows θ as a function of temperature for all particle types employed in this study. Here, the uncertainty in θ is mostly affected by the uncertainty in RH_{ice} and only to a lesser extent by J_{het}. For example, increasing J_{het} by 1 order of magnitude, leaving all other parameters the same, changes θ by ~0.3°. SRFA, O_3-exposed SRFA, and O_3-exposed leonardite particles
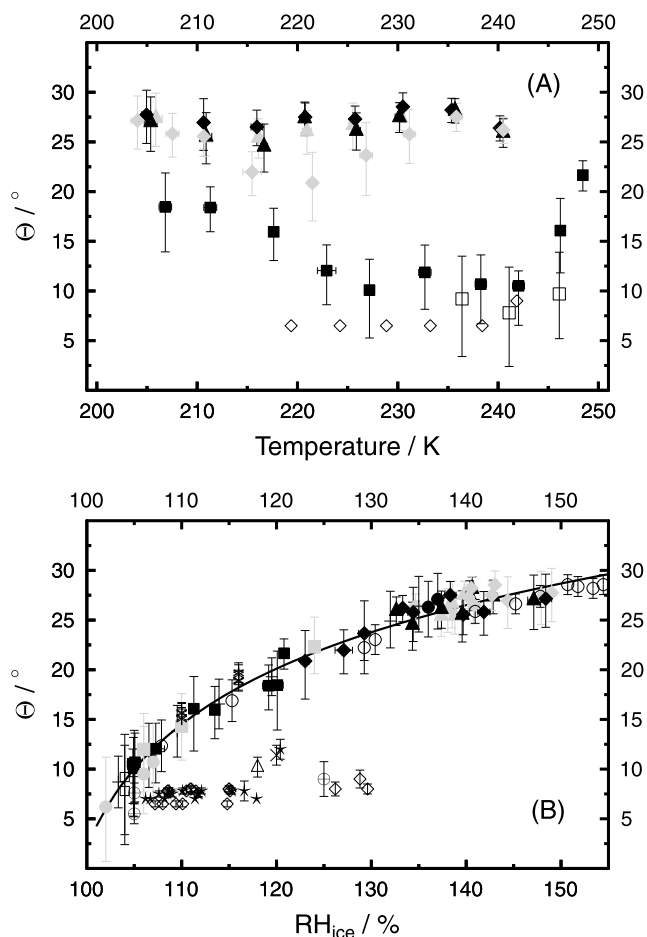
Figure 6. (a) The contact angle (θ) as a function of temperature for kaolinite (solid squares), leonardite (gray diamonds), O_3-exposed leonardite (black diamonds), SRFA (gray triangles), and O_3-exposed SRFA (black triangles). The θ data for kaolinite from previous studies by *Eastwood et al.* [2008] and *Welti et al.* [2009] are shown as open squares and open diamonds, respectively. (b) Plot of θ as a function of RH_{ice} for kaolinite (solid squares), leonardite (gray diamonds), O_3-exposed leonardite (black diamonds), SRFA (gray triangles), and O_3-exposed SRFA (black triangles) derived in this study and calcite (pluses), Muscovite (gray solid circles), montmorillonite (gray solid squares), kaolinite (open squares), and quartz (black solid circles) [*Eastwood et al.*, 2008], montmorillonite (stars) and kaolinite (open diamonds) [*Welti et al.*, 2009], Saharan dust and dust collected in Spain (asterisks) [*Kulkarni and Dobbie*, 2010], Arizona test dust (open circles) [*Kanji and Abbatt*, 2010], and Fe_2O_3 (circles with pluses), MgO (crosses), and SiO_2 (open triangles) [*Saunders et al.*, 2010]. Thin black line represents a logarithmic fit according to equation (8).

possess θ values of ~27°. Leonardite particles exhibit a wider range of θ from 20.9 to 27.5° and thus can serve as more efficient IN at temperatures from 215 to 227 K as indicated in Figure 4b. θ for kaolinite particles ranges from 10.1 to 21.7° at the observed temperatures in agreement with previously determined θ [*Eastwood et al.*, 2008; *Welti et al.*, 2009] as shown in Figure 6a. Overall the organic particles studied here exhibit larger θ values and thus are less efficient IN than kaolinite particles at temperature between 200 to 250 K.

[39] Figure 6b shows θ as a function of RH_{ice} for the particles employed in this study and previous deposition ice nucleation data for kaolinite, Arizona Test Dust, Muscovite, Montmorillonite, Quartz, Calcite, Saharan dust, dust collected in Spain, Fe_2O_3, MgO, and SiO_2 particles [*Eastwood et al.*, 2008; *Welti et al.*, 2009; *Kanji and Abbatt*, 2010; *Kulkarni and Dobbie*, 2010; *Saunders et al.*, 2010]. θ derived here and in previous studies [*Eastwood et al.*, 2008; *Kanji and Abbatt*, 2010; *Kulkarni and Dobbie*, 2010] show a very similar trend with RH_{ice} ice nucleation onsets and can be very well represented by

$$\theta = a + b \cdot \ln(RH_{ice} + c), \qquad (8)$$

where $a = -13.248$, $b = 10.4731$, $c = -95.785$, and RH_{ice} between 100% and 160%. The correlation coefficient, R^2, for this fit yields 0.98. It is remarkable that these different particle types which nucleate ice for a wide range of temperature and RH_{ice} onsets show a similar behavior with respect to RH_{ice} when expressed as θ. However, θ derived by *Welti et al.* [2009], and *Saunders et al.* [2010] deviate significantly from the other laboratory derived contact angles. The reason for this could lie in the different experimental techniques and methods to derive J_{het} and RH_{ice} necessary to calculate θ.

4. Atmospheric Implication

[40] Field measurements have shown that organic material can contribute a significant mass fraction to atmospheric aerosol particles [*Zhang et al.*, 2007]. Here we showed that SRFA, leonardite, and corresponding O_3-exposed particles can serve as IN for a wide range of temperatures and RH_{ice}. The observed onset conditions for cirrus cloud formation by *Ström et al.* [2003] and *Haag et al.* [2003] during the INCA (Interhemispheric differences in cirrus properties from anthropogenic emissions) field study and by *Heymsfield and Miloshevich* [1995] for continental cirrus are shown in Figure 4. *Haag et al.* [2003] reported ice formation in the Southern Hemisphere (SH) was initiated predominantly by homogeneous nucleation and in the Northern Hemisphere (NH) by homogeneous and selective heterogeneous nucleation. *Heymsfield and Miloshevich* [1995] derived bounds for the ice nucleation onset of cirrus clouds using field observations of quasi steady state orographic clouds and cirrus clouds. In addition, Figure 4 shows RH_{ice} thresholds for homogeneous ice nucleation of an aqueous droplet with 2.5 μm in diameter corresponding to a homogeneous ice nucleation rate coefficient of ~ 4×10^{10} cm^{-3} s^{-1} [*Koop et al.*, 2000].

[41] Figure 4 shows that the RH_{ice} ice nucleation onsets of SRFA and O_3-exposed SRFA particles via deposition mode are lower than those for homogeneous ice nucleation at $T_p <$ 235 K and are close to the lower bound of cirrus cloud onset conditions observed in the SH [*Haag et al.*, 2003; *Ström et al.*, 2003] suggesting that SRFA and O_3-exposed SRFA particles may act as IN under these conditions. Leonardite particles form ice at much lower RH_{ice} onsets compared to homogeneous ice nucleation. The observed RH_{ice} onsets of leonardite particles coincide in part with the observed cirrus

cloud onset conditions in the NH [*Haag et al.*, 2003; *Ström et al.*, 2003] and continental cirrus cloud formation [*Heymsfield and Miloshevich*, 1995]. However, O_3-exposed leonardite particles show ice nucleation onsets closer to the cirrus cloud onset conditions in the SH [*Ström et al.*, 2003]. The data presented here indicate that SRFA, O_3-exposed SRFA, leonardite, and O_3-exposed leonardite particles can initiate ice formation via heterogeneous ice nucleation under atmospheric conditions typically observed for cirrus formation.

[42] Initial water uptake and subsequent immersion freezing of SRFA, leonardite, and corresponding O_3-exposed particles at temperatures ≥ 236 K indicate that these particles can initiate ice formation relevant for the formation of mixed-phase clouds [*Prenni et al.*, 2009; *Verlinde et al.*, 2007]. Overall, ice nucleation data presented here suggest that HULIS-containing atmospheric particles have the potential to play a role in both cirrus and mixed-phase cloud formation irrespective of the degree of oxidation by O_3.

[43] The parameterization of θ with RH_{ice} allows estimation of J_{het} and ice crystal production rates (P_{ice}^{het}) when the cloud onset formation conditions are known. For this analysis, we assume θ to be independent of temperature in the temperature range for cloud activation. This is justified first by the experimental findings that θ does not change significantly within 10 K. Secondly, typical ice supersaturations for initiation of ice nucleation are achieved within a decrease of about 4 K in the temperature of the IN compared to the dew point of the surrounding environment [*Koop et al.*, 2000; *Murphy and Koop*, 2005]. For a particular ice nucleation onset the corresponding θ value can be read off Figure 6b and using equations (5), (6), and (7), J_{het} can be readily derived. If the available aerosol surface area per volume of air, A_p, is known, then $P_{ice}^{het} = A_p \cdot J_{het}$ in units of ice particles cm^{-3}(air) s^{-1}. The final maximum ice crystal concentrations are also constrained by the available water vapor and possible mass transfer due to the Wegener-Bergeron-Findeisen process [*Wegener*, 1911; *Bergeron*, 1935; *Findeisen*, 1938]. The proposed parameterization of θ, valid for a wide range of insoluble particles nucleating ice via deposition mode, and corresponding J_{het} derived as a function of T and RH_{ice} can be useful in applications such as cloud resolved modeling studies but also for post analysis of field observations to describe the evolution of the ice phase.

5. Summary

[44] The heterogeneous ice nucleation efficiency of laboratory generated kaolinite, leonardite, and SRFA particles was investigated as a function of temperature, relative humidity, nucleation mode, and O_3 exposure. Ice nucleation and water uptake were studied using a novel ice nucleation apparatus which allows control of particle temperature as low as 203 K and relative humidity up to water saturation. Validation of the new experimental setup was performed by determining the IN efficiency of kaolinite particles. The results corroborate that kaolinite particles are very efficient IN inducing ice nucleation via deposition mode at 102–124% RH_{ice} for temperatures between 207 and 251 K in agreement with previous studies.

[45] SRFA particles nucleated ice via deposition mode at 125–161% RH_{ice} for temperatures ≤ 230 K. At 236 and

241 K, ice formation occurred either via deposition mode or immersion freezing. At temperatures ≥ 246 K water uptake was first observed and followed by immersion freezing. The observed RH_{ice} ice nucleation onsets of SRFA particles are lower than those for homogeneous ice nucleation of aqueous droplets for temperatures below 231 K [*Koop et al.*, 2000] and close to the observed lower bound of cirrus cloud onset conditions typical for the Southern Hemisphere [*Haag et al.*, 2003; *Ström et al.*, 2003]. Leonardite particles nucleated ice via deposition mode at 112–162% RH_{ice} for temperatures ≤ 241 K and at higher temperature water uptake and in some cases subsequent immersion freezing was observed. The observed RH_{ice} ice nucleation onsets of leonardite particles coincide in part with the cirrus onset conditions observed in the Northern Hemisphere [*Haag et al.*, 2003; *Ström et al.*, 2003] and continental cirrus cloud formation [*Heymsfield and Miloshevich*, 1995].

[46] O_3-exposed SRFA particles nucleated ice via deposition mode at temperatures ≤ 241 K indicating that oxidation by O_3 can enhance the ice nucleation efficiency. But at temperatures ≤ 231 K ice nucleation occurred on O_3-exposed SRFA particles at similar RH_{ice} ice nucleation onsets as for SRFA particles. O_3-exposed leonardite particles nucleated ice via deposition mode at 131–162% RH_{ice} for temperatures ≤ 236 K. At 241 K, ice formation occurred either via deposition mode or immersion freezing on O_3-exposed leonardite particles and at higher-temperature water uptake and in some cases subsequent immersion freezing were observed. O_3-exposed leonardite particles nucleated ice in average 10–20% RH_{ice} higher compared to unexposed leonardite particles for temperatures between 215 and 227 K suggesting that oxidation by O_3 renders leonardite particles less efficient IN in this temperature range. These results indicate that particle oxidation by O_3 may have different impacts on the ice nucleation efficiency of the organic particles studied here. More ice nucleation studies taking into account particle oxidation by atmospheric trace gases are needed to assess its importance on the ice nucleation efficiency of organic particles.

[47] We have shown that SRFA, leonardite, and corresponding O_3-exposed particles can nucleate ice via deposition mode at atmospheric conditions typical for cirrus cloud formation. Immersion freezing induced by SRFA, leonardite and corresponding O_3-exposed particles at temperatures >236 K indicates that these organic particles can induce ice formation at atmospheric conditions relevant for mixed-phase clouds. Our results suggest that HULIS-containing particles can play important roles in both cirrus and mixed-phase cloud formation processes.

[48] Experimentally derived heterogeneous ice nucleation rate coefficients were applied to calculate contact angles using classical nucleation theory. The contact angles determined here and from previous studies representing various types of IN demonstrate a very similar behavior as a function of RH_{ice} ice nucleation onsets. A parameterization of contact angle as a function of RH_{ice} ice nucleation onsets was derived which allows determination of the corresponding heterogeneous ice nucleation rate coefficients assuming that the contact angle does not change within the temperature range of cloud activation. This yields, if onset conditions for cloud formation are known, ice crystal production rates and corresponding ice crystal number con-

centrations for deposition ice nucleation. The proposed deposition ice nucleation parameterization can provide a valuable tool for post analysis of observed atmospheric ice crystal formation for a wide range of different IN and for application in cloud-resolving modeling studies.

References

Albrecht, B. (1989), Aerosols, cloud microphysics and fractional cloudiness, *Science*, 245, 1227–1230, doi:10.1126/science.245.4923.1227.

Avramov, A., and J. Y. Harrington (2010), Influence of parameterized ice habit on simulated mixed phase Arctic clouds, *J. Geophys. Res.*, 115, D03205, doi:10.1029/2009JD012108.

Baduel, C., D. Voisin, and J. L. Jaffrezo (2009), Comparison of analytical methods for humic like substances (HULIS) measurements in atmospheric particles, *Atmos. Chem. Phys.*, 9(16), 5949–5962, doi:10.5194/acp-9-5949-2009.

Bailey, M., and J. Hallett (2002), Nucleation effects on the habit of vapour grown ice crystals from −18°C to −42°C, *Q. J. R. Meteorol. Soc.*, 128, 1461–1483, doi:10.1002/qj.200212858304.

Bailey, M., and J. Hallett (2004), Growth rates and habits of ice crystals between −20°C and −70°C, *J. Atmos. Sci.*, 61(5), 514–544, doi:10.1175/1520-0469(2004)061<0514:GRAHOI>2.0.CO;2.

Baker, M. B. (1997), Cloud microphysics and climate, *Science*, 276, 1072–1078, doi:10.1126/science.276.5315.1072.

Baker, M. B., and T. Peter (2008), Small-scale cloud processes and climate, *Nature*, 451, 299–300, doi:10.1038/nature06594.

Bergeron, T. (1935), On the physics of clouds and precipitation, paper presented at 5th Assembly, Int. Union of Geod. and Geophys., Lisbon.

Brooks, S. D., P. J. DeMott, and S. M. Kreidenweis (2004), Water uptake by particles containing humic materials and mixtures of humic materials with ammonium sulfate, *Atmos. Environ.*, 38(13), 1859–1868, doi:10.1016/j.atmosenv.2004.01.009.

Cantrell, W., and A. Heymsfield (2005), Production of ice in tropospheric clouds, *Bull. Am. Meteorol. Soc.*, 86(6), 795–807, doi:10.1175/BAMS-86-6-795.

Cavalli, F., et al. (2004), Advances in characterization of size-resolved organic matter in marine aerosol over the North Atlantic, *J. Geophys. Res.*, 109, D24215, doi:10.1029/2004JD005137.

Chan, M. N., and C. K. Chan (2003), Hygroscopic properties of two model humic-like substances and their mixtures with inorganics of atmospheric importance, *Environ. Sci. Technol.*, 37(22), 5109–5115, doi:10.1021/es034272o.

Chen, J., A. Hazra, and Z. Levin (2008), Parameterizing ice nucleation rates using contact angle and activation energy derived from laboratory data, *Atmos. Chem. Phys.*, 8(24), 7431–7449, doi:10.5194/acp-8-7431-2008.

Chen, T., W. B. Rossow, and Y. Zhang (2000), Radiative effects of cloud-type variations, *J. Clim.*, 13, 264–286, doi:10.1175/1520-0442(2000)013<0264:REOCTV>2.0.CO;2.

Chen, Y., S. M. Kreidenweis, L. M. McInnes, D. C. Rogers, and P. J. DeMott (1998), Single particle analyses of ice nucleating aerosols in the upper troposphere and lower stratosphere, *Geophys. Res. Lett.*, 25(9), 1391–1394, doi:10.1029/97GL03261.

Choi, Y. S., and C. H. Ho (2006), Radiative effect of cirrus with different optical properties over the tropics in MODIS and CERES observations, *Geophys. Res. Lett.*, 33, L21811, doi:10.1029/2006GL027403.

Curry, J. A., J. L. Schramm, W. B. Rossow, and D. Randall (1996), Overview of arctic cloud and radiation characteristics, *J. Clim.*, 9, 1731–1764, doi:10.1175/1520-0442(1996)009<1731:OOACAR>2.0.CO;2.

Cziczo, D. J., D. M. Murphy, P. K. Hudson, and D. S. Thomson (2004), Single particle measurements of the chemical composition of cirrus ice residue during CRYSTAL-FACE, *J. Geophys. Res.*, 109, D04201, doi:10.1029/2003JD004032.

D'Anna, B., J. Adla, G. Christian, S. Konrad, F. Simon, A. Markus, and W. Armin (2009), Light-induced ozone depletion by humic acid films and submicron aerosol particles, *J. Geophys. Res.*, 114, D12301, doi:10.1029/2008JD011237.

Decesari, S., M. C. Facchini, E. Matta, M. Mircea, S. Fuzzi, A. R. Chughtai, and D. M. Smith (2002), Water soluble organic compounds formed by oxidation of soot, *Atmos. Environ.*, 36(11), 1827–1832, doi:10.1016/S1352-2310(02)00141-3.

DeMott, P. J., D. J. Cziczo, A. J. Prenni, D. M. Murphy, S. M. Kreidenweis, D. S. Thomson, R. Borys, and D. C. Rogers (2003), Measurements of the concentration and composition of nuclei for cirrus formation, *Proc. Natl. Acad. Sci. U. S. A.*, 100(25), 14,655–14,660, doi:10.1073/pnas.2532677100.

Dinar, E., I. Taraniuk, E. R. Graber, S. Katsman, T. Moise, T. Anttila, T. F. Mentel, and Y. Rudich (2006), Cloud condensation nuclei properties of model and atmospheric HULIS, *Atmos. Chem. Phys.*, 6(9), 2465–2482, doi:10.5194/acp-6-2465-2006.

Dymarska, M., B. J. Murray, L. M. Sun, M. L. Eastwood, D. A. Knopf, and A. K. Bertram (2006), Deposition ice nucleation on soot at temperatures relevant for the lower troposphere, *J. Geophys. Res.*, 111, D04204, doi:10.1029/2005JD006627.

Eastwood, M. L., S. Cremel, C. Gehrke, E. Girard, and A. K. Bertram (2008), Ice nucleation on mineral dust particles: Onset conditions, nucleation rates and contact angles, *J. Geophys. Res.*, 113, D22203, doi:10.1029/2008JD010639.

Eliason, T. L., S. Aloisio, D. J. Donaldson, D. J. Cziczo, and V. Vaida (2003), Processing of unsaturated organic acid films and aerosols by ozone, *Atmos. Environ.*, 37(16), 2207–2219, doi:10.1016/S1352-2310(03)00149-3.

Facchini, M. C., M. Mircea, S. Fuzzi, and R. J. Charlson (1999), Cloud albedo enhancement by surface-active organic solutes in growing droplets, *Nature*, 401(6750), 257–259, doi:10.1038/45758.

Feczko, T., H. Puxbaum, A. Kasper-Giebl, M. Handler, A. Limbeck, A. Gelencsér, C. Pio, S. Preunkert, and M. Legrand (2007), Determination of water and alkanline extractable atmospheric humic-like substances with the TU Vienna HULIS analyzer in samples from six background sites in Europe, *J. Geophys. Res.*, 112, D23S10, doi:10.1029/2006JD008331.

Findeisen, W. (1938), Die kolloidmeteorologischen Vorgänge bei der Niederschlagsbildung (colloidal meteorological processes in the formation of precipitation), *Meteorol. Z.*, 55, 121–133.

Fletcher, N. (1958), Size effect in heterogeneous nucleation, *J. Chem. Phys.*, 29, 572–576, doi:10.1063/1.1744540.

Fornea, A. P., S. D. Brooks, J. B. Dooley, and A. Saha (2009), Heterogeneous freezing of ice on atmospheric aerosols containing ash, soot, and soil, *J. Geophys. Res.*, 114, D13201, doi:10.1029/2009JD011958.

Forster, P., et al. (2007), Changes in atmospheric constituents and in radiative forcing, in *Climate Change 2007: The Physical Science Basis. Contribution of Working Group I to the Fourth Assessment Report of the Intergovernmental Panel on Climate Change*, edited by S. Solomon et al., pp. 131–234, Cambridge Univ. Press, Cambridge, U. K.

Froyd, K. D., D. M. Murphy, P. Lawson, D. Baumgardner, and R. L. Herman (2010), Aerosols that form subvisible cirrus at the tropical tropopause, *Atmos. Chem. Phys.*, 10(1), 209–218, doi:10.5194/acp-10-209-2010.

Garten, V. A., and R. B. Head (1964), Carbon particles and ice nucleation, *Nature*, 201, 1091–1092, doi:10.1038/2011091a0.

Graber, E. R., and Y. Rudich (2006), Atmospheric HULIS: How humic-like are they? A comprehensive and critical review, *Atmos. Chem. Phys.*, 6(3), 729–753, doi:10.5194/acp-6-729-2006.

Gysel, M., E. Weingartner, S. Nyeki, D. Paulsen, U. Baltensperger, I. Galambos, and G. Kiss (2004), Hygroscopic properties of water-soluble matter and humic-like organics in atmospheric fine aerosol, *Atmos. Chem. Phys.*, 4(13), 35–50, doi:10.5194/acp-4-35-2004.

Haag, W., B. Kärcher, J. Ström, A. Minikin, U. Lohmann, J. Ovarlez, and A. Stohl (2003), Freezing thresholds and cirrus cloud formation mechanisms inferred from in situ measurements of relative humidity, *Atmos. Chem. Phys.*, 3(5), 1791–1806, doi:10.5194/acp-3-1791-2003.

Hartmann, D. L., M. E. Ockert-Bell, and M. L. Michelsen (1992), The effect of cloud type on earth's energy balance: Global analysis, *J. Clim.*, 5, 1281–1304, doi:10.1175/1520-0442(1992)005<1281:TEOCTO>2.0.CO;2.

Heymsfield, A. J., and L. M. Miloshevich (1995), Relative humidity and temperature influences on cirrus formation and evolution: Observations from wave clouds and FIRE II, *J. Atmos. Sci.*, 52(23), 4302–4326, doi:10.1175/1520-0469(1995)052<4302:RHATIO>2.0.CO;2.

Hung, H. M., Y. Katrib, and S. T. Martin (2005), Products and mechanisms of the reaction of oleic acid with ozone and nitrate radical, *J. Phys. Chem. A*, 109(20), 4517–4530, doi:10.1021/jp0500900.

Jang, M. S., N. M. Czoschke, S. Lee, and R. M. Kamens (2002), Heterogeneous atmospheric aerosol production by acid-catalyzed particle-phase reactions, *Science*, 298, 814–817, doi:10.1126/science.1075798.

Jost, H. J., et al. (2004), In-situ observations of mid-latitude forest fire plumes deep in the stratosphere, *Geophys. Res. Lett.*, 31, L11101, doi:10.1029/2003GL019253.

Kanakidou, M., et al. (2005), Organic aerosol and global climate modelling: A review, *Atmos. Chem. Phys.*, 5(4), 1053–1123, doi:10.5194/acp-5-1053-2005.

Kanji, Z. A., and J. P. D. Abbatt (2006), Laboratory studies of ice formation via deposition mode nucleation onto mineral dust and n-hexane soot samples, *J. Geophys. Res.*, *111*, D16204, doi:10.1029/2005JD006766.

Kanji, Z. A., and J. P. D. Abbatt (2010), Ice nucleation onto Arizona test dust at cirrus temperatures: Effenct of temperature and aerosol size on onset relative humidity, *J. Phys. Chem. A*, *114*, 935–941, doi:10.1021/jp908661m.

Kanji, Z. A., O. Florea, and J. P. D. Abbatt (2008), Ice formation via deposition nucleation on mineral dust and organics: Dependence of onset relative humidity on total particulate surface area, *Environ. Res. Lett.*, *3*(2), 025004, doi:10.1088/1748-9326/3/2/025004.

Kärcher, B. (1998), Physicochemistry of aircraft-generated liquid aerosols, soot, and ice particles: 1. Model description, *J. Geophys. Res.*, *103*(D14), 17,111–17,128, doi:10.1029/98JD01044.

Kärcher, B., and J. Ström (2003), The roles of dynamical variability and aerosols in cirrus cloud formation, *Atmos. Chem. Phys.*, *3*(3), 823–838, doi:10.5194/acp-3-823-2003.

Kiss, G., E. Tombacz, and H. C. Hansson (2005), Surface tension effects of humic-like substances in the aqueous extract of tropospheric fine aerosol, *J. Atmos. Chem.*, *50*(3), 279–294, doi:10.1007/s10874-005-5079-5.

Knopf, D. A., and T. Koop (2006), Heterogeneous nucleation of ice on surrogates of mineral dust, *J. Geophys. Res.*, *111*, D12201, doi:10.1029/2005JD006894.

Knopf, D. A., and M. D. Lopez (2009), Homogeneous ice freezing temperatures and ice nucleation rates of aqueous ammonium sulfate and aqueous levoglucosan particles for relevant atmospheric conditions, *Phys. Chem. Chem. Phys.*, *11*, 8056–8068, doi:10.1039/b903750k.

Knopf, D. A., T. Koop, B. P. Luo, U. G. Weers, and T. Peter (2002), Homogeneous nucleation of NAD and NAT in liquid stratospheric aerosols: Insufficient to explain denitrification, *Atmos. Chem. Phys.*, *2*(3), 207–214, doi:10.5194/acp-2-207-2002.

Knopf, D. A., L. M. Anthony, and A. K. Bertram (2005), Reactive uptake of O3 by multicomponent and multiphase mixtures containing oleic acid, *J. Phys. Chem. A*, *109*, 5579–5589, doi:10.1021/jp0512513.

Knopf, D. A., J. Mak, S. Gross, and A. K. Bertram (2006), Does atmospheric processing of saturated hydrocarbon surfaces by NO3 lead to volatilization?, *Geophys. Res. Lett.*, *33*, L17816, doi:10.1029/2006GL026884.

Knopf, D. A., B. Wang, A. Laskin, R. C. Moffet, and M. K. Gilles (2010), Heterogeneous nucleation of ice on anthropogenic organic particles collected in Mexico City, *Geophys. Res. Lett.*, *37*, L11803, doi:10.1029/2010GL043362.

Koehler, K. A., P. J. DeMott, S. M. Kreidenweis, O. B. Popovicheva, M. D. Petters, C. M. Carrico, E. D. Kireeva, T. D. Khokhlovac, and N. K. Shonijac (2009), Cloud condensation nuclei and ice nucleation activity of hydrophobic and hydrophilic soot particles, *Phys. Chem. Chem. Phys.*, *11*, 7906–7920, doi:10.1039/b905334b.

Koop, T., B. P. Luo, U. M. Biermann, P. J. Crutzen, and T. Peter (1997), Freezing of HNO3/H2SO4/H2O solutions at stratospheric temperatures: Nucleation statistics and experiments, *J. Phys. Chem. A*, *101*, 1117–1133.

Koop, T., H. P. Ng, L. T. Molina, and M. J. Molina (1998), A new optical technique to study aerosol phase transitions: The nucleation of ice from H2SO4 aerosols, *J. Phys. Chem. A*, *102*, 8924–8931, doi:10.1021/jp9828078.

Koop, T., B. P. Luo, A. Tsias, and T. Peter (2000), Water activity as the determinant for homogeneous ice nucleation in aqueous solutions, *Nature*, *406*, 611–614, doi:10.1038/35020537.

Krivacsy, Z., A. Hoffer, Z. Sarvari, D. Temesi, U. Baltensperger, S. Nyeki, E. Weingartner, S. Kleefeld, and S. G. Jennings (2001), Role of organic and black carbon in the chemical composition of atmospheric aerosol at European background sites, *Atmos. Environ.*, *35*, 6231–6244, doi:10.1016/S1352-2310(01)00467-8.

Kulkarni, G., and S. Dobbie (2010), Ice nucleation properties of mineral dust particles: Determination of onset rh_i, in active fraction, nucleation time-lag, and the effect of active sites on contact angles, *Atmos. Chem. Phys.*, *10*(1), 95–105, doi:10.5194/acp-10-95-2010.

Lee, J., P. Yang, A. E. Dessler, B.-C. Gao, and S. Platnick (2009), Distribution and radiative forcing of tropical thin cirrus clouds, *J. Atmos. Sci.*, *66*(12), 3721–3731, doi:10.1175/2009JAS3183.1.

Li, S. M., J. Tang, H. S. Xue, and D. Toom-Sauntry (2000), Size distribution and estimated optical properties of carbonate, water soluble organic carbon, and sulfate in aerosols at a remote high altitude site in western China, *Geophys. Res. Lett.*, *27*, 1107–1110, doi:10.1029/1999GL010929.

Lin, P., X. Huang, L. He, and J. Z. Yu (2010a), Abundance and size distribution of HULIS in ambient aerosols at a rural site in south China, *J. Aerosol. Sci.*, *41*, 74–87, doi:10.1016/j.jaerosci.2009.09.001.

Lin, P., G. Engling, and J. Z. Yu (2010b), Humic-like substances in fresh emissions of rice straw burning and in ambient aerosols in the Pearl River delta region, China, *Atmos. Chem. Phys.*, *10*(14), 6487–6500, doi:10.5194/acp-10-6487-2010.

Lohmann, U., and J. Feichter (2005), Global indirect aerosol effects: A review, *Atmos. Chem. Phys.*, *5*(3), 715–737, doi:10.5194/acp-5-715-2005.

Lukács, H., et al. (2007), Seasonal trends and possible sources of brown carbon based on 2-year aerosol measurements at six sites in Europe, *J. Geophys. Res.*, *112*, D23S18, doi:10.1029/2006JD008151.

Lynch, D. K., K. Sassen, D. O. Starr, and G. Stephens (2002), *Cirrus*, Oxford Univ. Press, New York.

Mayol-Bracero, O. L., P. Guyon, B. Graham, G. Roberts, M. O. Andreae, S. Decesari, M. C. Facchini, S. Fuzzi, and P. Artaxo (2002), Water-soluble organic compounds in biomass burning aerosols over Amazonia: 2. Apportionment of the chemical composition and importance of the polyacidic fraction, *J. Geophys. Res.*, *107*(D20), 8091, doi:10.1029/2001JD000522.

McFarquhar, G. M., G. Zhang, M. R. Poellot, G. L. Kok, R. McCoy, T. Tooman, A. Fridlind, and A. J. Heymsfield (2007), Ice properties of single-layer stratocumulus during the Mixed-Phase Arctic Cloud Experiment: 1. Observations, *J. Geophys. Res.*, *112*, D24201, doi:10.1029/2007jd008633.

McFiggans, G., et al. (2006), The effect of physical and chemical aerosol properties on warm cloud droplet activation, *Atmos. Chem. Phys.*, *6*(9), 2593–2649, doi:10.5194/acp-6-2593-2006.

Molina, M. J., A. V. Ivanov, S. Trakhtenberg, and L. T. Molina (2004), Atmospheric evolution of organic aerosol, *Geophys. Res. Lett.*, *31*, L22104, doi:10.1029/2004GL020910.

Morrison, H., J. Curry, and V. I. Khvorostyanov (2005), A new double-moment microphysics parameterization for application in cloud and climate models. Part I: Description, *J. Atmos. Sci.*, *62*, 1665–1677, doi:10.1175/JAS3446.1.

Murphy, D. M., and T. Koop (2005), Review of the vapour pressures of ice and supercooled water for atmospheric applications, *Q. J. R. Meteorol. Soc.*, *131*(608), 1539–1565, doi:10.1256/qj.04.94.

Murphy, D. M., D. S. Thomson, and T. M. J. Mahoney (1998), In situ measurements of organics, meteoritic material, mercury, and other elements in aerosols at 5 to 19 kilometers, *Science*, *282*, 1664–1669, doi:10.1126/science.282.5394.1664.

Murphy, D. M., D. J. Cziczo, P. K. Hudson, and D. S. Thomson (2007), Carbonaceous material in aerosol particles in the lower stratosphere and tropopause region, *J. Geophys. Res.*, *112*, D04203, doi:10.1029/2006JD007297.

Parsons, M. T., J. Mak, S. R. Lipetz, and A. K. Bertram (2004), Deliquescence of malonic, succinic, glutaric, and adipic acid particles, *J. Geophys. Res.*, *109*, D06212, doi:10.1029/2003JD004075.

Prenni, A., P. J. DeMott, S. M. Kreidenweis, J. Y. Harrington, A. Avramov, J. Verlinde, M. Tjernström, C. N. Long, and P. Q. Olsson (2007), Can ice-nucleating aerosols affect arctic seasonal climate?, *Bull. Am. Meteorol. Soc.*, *88*(4), 541–550, doi:10.1175/BAMS-88-4-541.

Prenni, A. J., P. J. Demott, D. C. Rogers, S. M. Kreidenweis, G. M. McFarquhar, G. Zhang, and M. R. Poellot (2009), Ice nuclei characteristics from M-PACE and their relation to ice formation in clouds, *Tellus, Ser. B*, *61*(2), 436–448, doi:10.1111/j.1600-0889.2009.00415.x.

Pruppacher, R. H., and J. D. Klett (1997), *Microphysics of Clouds and Precipitation*, Kluwer Acad., Dordrecht, Netherlands.

Ramanathan, V., P. J. Crutzen, J. T. Kiehl, and D. Rosenfeld (2001), Aerosols, climate, and the hydrological cycle, *Science*, *294*, 2119–2124, doi:10.1126/science.1064034.

Roberts, P., and J. Hallett (1968), A laboratory study of the ice nucleating properties of some mineral particulates, *Q. J. R. Meteorol. Soc.*, *94*, 25–34, doi:10.1002/qj.49709439904.

Rosenfeld, D. (2000), Suppression of rain and snow by urban and industrial air pollution, *Science*, *287*, 1793–1796, doi:10.1126/science.287.5459.1793.

Rudich, Y. (2003), Laboratory perspectives on the chemical transformations of organic matter in atmospheric particles, *Chem. Rev.*, *103*(12), 5097–5124, doi:10.1021/cr020508f.

Rudich, Y., N. M. Donahue, and T. F. Mentel (2007), Aging of organic aerosol: Bridging the gap between laboratory and field studies, *Annu. Rev. Phys. Chem.*, *58*, 321–352, doi:10.1146/annurev.physchem.58.032806.104432.

Salam, A., U. Lohmann, B. Crenna, G. Lesins, P. Klages, D. Rogers, R. Irani, A. MacGillivray, and M. Coffin (2006), Ice nucleation studies of mineral dust particles with a new continuous flow diffusion chamber, *Aerosol Sci. Technol.*, *40*(2), 134–143, doi:10.1080/02786820500444853.

Salma, I., R. Ocskay, and G. G. Láng (2008), Properties of atmospheric humic-like substances—Water system, *Atmos. Chem. Phys.*, *8*(8), 2243–2254, doi:10.5194/acp-8-2243-2008.

Saunders, R. W., et al. (2010), An aerosol chamber investigation of the heterogeneous ice nucleating potential of refractory nanoparticles, *Atmos. Chem. Phys.*, *10*(3), 1227–1247, doi:10.5194/acp-10-1227-2010.

Schaller, R. C., and N. Fukuta (1979), Ice nucleation by aerosol particles: Experimental studies using a wedge-shaped ice thermal diffusion chamber, *J. Atmos. Sci.*, *36*, 1788–1802, doi:10.1175/1520-0469(1979) 036<1788:INBAPE>2.0.CO;2.

Springmann, M., D. A. Knopf, and N. Riemer (2009), Detailed heterogeneous chemistry in an urban plume box model: Reversible co-adsorption of O_3, NO_2, and H_2O on soot coated with benzo[a]pyrene, *Atmos. Chem. Phys.*, *9*(19), 7461–7479, doi:10.5194/acp-9-7461-2009.

Ström, J., et al. (2003), Cirrus cloud occurrence as function of ambient relative humidity: A comparison of observations obtained during the INCA experiment, *Atmos. Chem. Phys.*, *3*(5), 1807–1816, doi:10.5194/acp-3-1807-2003.

Svenningsson, B., J. Rissler, E. Swietlicki, M. Mircea, M. Bilde, M. C. Facchini, S. Decesari, S. Fuzzi, J. Zhou, J. Monster, and T. Rosenorn (2006), Hygroscopic growth and critical supersaturations for mixed aerosol particles of inorganic and organic compounds of atmospheric relevance, *Atmos. Chem. Phys.*, *6*(9), 1937–1952, doi:10.5194/acp-6-1937-2006.

Thomas, E. R., G. J. Frost, and Y. Rudich (2001), Reactive uptake of ozone by proxies for organic aerosols: Surface-bound and gas-phase products, *J. Geophys. Res.*, *106*(D3), 3045–3056, doi:10.1029/2000JD900595.

Twomey, S. (1974), Pollution and planetary albedo, *Atmos. Environ.*, *8*(12), 1251–1256, doi:10.1016/j.atmosenv.2007.10.062.

Vali, G. (1985), Nucleation terminology, *J. Aerosol Sci.*, *16*(6), 575–576, doi:10.1016/0021-8502(85)90009-6.

Vavrus, S. (2004), The impact of cloud feedbacks on arctic climate under greenhouse forcing, *J. Clim.*, *17*, 603–615, doi:10.1175/1520-0442 (2004)017<0603:TIOCFO>2.0.CO;2.

Verlinde, J., et al. (2007), The mixed-phase arctic cloud experiment, *Bull. Am. Meteorol. Soc.*, *88*(2), 205–221, doi:10.1175/BAMS-88-2-205.

Wegener, A. (1911), *Thermodynamik der Atmosphäre*, Johann Ambrosius Barth, Leipzig, Germany.

Welti, A., F. Lüönd, and U. Lohmann (2009), Influence of particle size on the ice nucleating ability of mineral dusts, *Atmos. Chem. Phys.*, *9*(18), 6705–6715, doi:10.5194/acp-9-6705-2009.

Wendisch, M., P. Yang, and P. Pilewskie (2007), Effects of ice crystal habit on thermal infrared radiative properties and forcing of cirrus, *J. Geophys. Res.*, *112*, D08201, doi:10.1029/2006JD007899.

Wylie, D. P., W. P. Jackson, W. P. Menzel, and J. J. Bates (2005), Trends in global cloud cover in two decades of HIRS observations, *J. Clim.*, *18*, 3021–3031, doi:10.1175/JCLI3461.1.

Ye, T., D. Wynn, R. Dudek, and E. Borguet (2001), Photoreactivity of alkylsiloxane self-assembled monolayers on silicon oxide surfaces, *Langmuir*, *17*, 4497–4500, doi:10.1021/la010697h.

Zahardis, J., and G. A. Petrucci (2007), The oleic acid-ozone heterogeneous reaction system: Products, kinetics, secondary chemistry, and atmospheric implications of a model system—A review, *Atmos. Chem. Phys.*, *7*, 1237–1274.

Zhang, Q., et al. (2007), Ubiquity and dominance of oxygenated species in organic aerosols in anthropogenically-influenced Northern Hemisphere midlatitudes, *Geophys. Res. Lett.*, *34*, L13801, doi:10.1029/ 2007GL029979.

Zimmermann, F., M. Ebert, A. Worringen, L. Schutz, and S. Weinbruch (2007), Environmental scanning electron microscopy (ESEM) as a new technique to determine the ice nucleation capability of individual atmospheric aerosol particles, *Atmos. Environ.*, *41*(37), 8219–8227, doi:10.1016/j.atmosenv.2007.06.023.

Zobrist, B., T. Koop, B. P. Luo, C. Marcolli, and T. Peter (2007), Heterogeneous ice nucleation rate coefficient of water droplets coated by a non-adecanol monolayer, *J. Phys. Chem. A*, *111*, 2149–2155.

D. A. Knopf and B. Wang, Institute for Terrestrial and Planetary Atmospheres, School of Marine and Atmospheric Sciences, State University of New York at Stony Brook, Stony Brook, NY 11794, USA. (daniel.knopf@stonybrook.edu)